Specific sample configuration for studying photogenerated electron transfer at the semiconductor/water interface by Electron Paramagnetic Resonance

Pablo Abarca Martinez, Marc Basler, Laurène Youssef, Cédric Jaoul, Patrice Valorge, Nolwenn Le Breton, Bertrand Vileno, David Martel, François Courtier

Specific sample configuration for studying photogenerated electron transfer at the semiconductor/water interface by Electron Paramagnetic Resonance

Pablo Abarca Martinez[c], Marc Basler[a], François Courtier[a], Laurène Youssef[c], Cédric Jaoul[c], Patrice Valorge[c], Nolwenn Le Breton[b], Bertrand Vileno[b*], David Martel[a*]*

[a] Université de Strasbourg, CNRS, Institut Charles Sadron (ICS), UPR 22, F-67000 Strasbourg, France. E mail david.martel@ics-cnrs.unistra.fr

[b] Université de Strasbourg, CNRS, Institut de Chimie, UMR 7177, F-67081 Strasbourg, France. E mail bertrand.vileno@unistra.fr

[c] Université de Limoges, CNRS, Institut de Rechercher sur les Céramiques (IRCER), UMR 7315, 12 rue Atlantis Limoges, France. E mail cedric.jaoul@unilim.fr

Abstract

Photogeneration of electrons from amorphous phase and anatase phase thin films of titanium oxide in contact with water was monitored by Electron Paramagnetic Resonance. The semiconducting oxide thin films were deposited on glass fibers of 250 µm diameter by Reactive Magnetron Sputtering and were centered inside capillaries of ca. 1 mm diameter filled with aqueous solution of a paramagnetic probe molecule. This proof of concept, non-restrictive to titanium oxide, makes it possible to reuse of the same fiber for multiple measurements and, as it respects the cylindrical symmetry, it should provide mechanistic investigations with reliable and quantifiable data on photogenerated electron transfer at the semiconductor/water interface.

I. Introduction

Since the industrial revolution in the early 19th century, the massive use of primary fossil energy resources, to produce electric, thermic or mechanical energy inevitably led to their rarefaction. Therefore, an energy crisis in the near future is unavoidable, together with air pollution, which contributes to the global warming [1]. Consequently, additionally to limit the energy use, novel carbon-free paths involving others types of primary energies have to be developed. This is the kind of challenges we are facing: replacing oil, coal and gas with other primary energies avoiding pollutions, at least during use. Nuclear, geothermal and sun power are primary energy sources (biomass, hydroelectric and wind power deriving from solar energy). Solar energy is perhaps the most promising, as it is present all over the planet yet being intermittent. While energy storage devices set to improve in the coming years, solar energy could be one of the

solutions to consider. As for an example, in the field of electric production, photovoltaic systems, including solar photovoltaic power plants, are already in widespread use. However, particular attention must be paid to the ratio energy expended to build the devices. Energy finally harvested while considering the inherent limited efficiency can hinder future developments.

For several decades, another approach has been envisaged focusing on the generation of a potentially powerful energy vector: the dihydrogen (H_2). This molecule can be used to produce e-fuel (synthetic fuels) [2] or electricity. For instance, the recombination of H_2 and O_2, in a fuel cell, was used to generate electricity for the Apollo rockets. So far, there are two main ways to generate H_2: steam reforming and electrolysis. The first one mentioned uses methane, whose impact on the greenhouse effect is worse than that of carbon dioxide. The later cited requires the expenditure of a large amount of energy from power stations to produce H_2, so the energy efficiency is therefore questionable. Since 1972, it is known that H_2 can be generated when exciting titanium oxide (TiO_2) semiconductors (SC) with light [3] and the use of the free solar energy then became a challenge and despite 50 years of in-depth studies, machine performance has been rather mediocre. Two main reasons can explain such observation. On the one hand, the optimization of the chemical nature, shape and size of the material to ensure an optimal utilization of the solar spectrum and the best yield. These points can be treated either experimentally [4-6] or by calculation [7]. On the other hand, the modest efficiency can also be attributed to a lack of knowledge of SC/water interfacial charge transfer processes [8-10]. The present work ensues on the second observation while focusing on a better understanding of the interfacial processes involved in the H_2 photogeneration. We are developing a novel methodology, based on Electron Paramagnetic Resonance (EPR) to provide reliable data for probing and modeling interfacial processes [11]. In previous work, we studied suspensions of titanium oxide (TiO_2) nanoparticles (NPs) highlighting intrinsic limitations inherent from such yet classically used *modus operandi* [12]. Following this, we investigated TiO_2 NPs/polyelectrolyte-based hybrid films deposited on internal wall of submillimeter glass capillaries, which still exhibited constraints preventing from obtaining fully reliable data [11]. A classical pitfall when using nanoobjects-based materials is their variability in terms of system parameters (size, shape, crystallinity, …). While it may be fitted for industrial applications, it is hardly suitable for basic investigations. Depending of the approach, specific objects of study need to be adapted (e.g. surface roughness in near field microscopies studies). In our case, we have to respect two constraints: the geometry and the dimension of the device. Due to H_2O

dielectric constant, the use of aqueous solution in EPR require peculiar geometry in terms of thickness of the probed solvent being ≤ 1 mm. Consequently, cylindrical geometry has been chosen with 1 mm diameter size glass capillary. The present work displays a novel configuration for EPR cell, enabling work with model SC configuration in line with EPR measurements, electron photogeneration, quantification (kinetic constants) and modeling (competition between several molecules and different mechanisms) by a SC in contact with an aqueous environment. The EPR cell configuration is based on covering a glass fiber of 250 µm diameter with a thin TiO_2 oxide film (amorphous or anatase structure) prepared by Reactive Magnetron Sputtering. This fiber is inserted and centered inside capillaries of 1mm diameter which is filled with a solution of paramagnetic probe (4-hydroxy-2,2,6,6-tetramethylpiperidin-1-oxyl: TEMPOL), The principle of the EPR measurements is to follow the evolution of the TEMPOL EPR signal as a function of illumination time as it can be reduced either by small radicals [13] or by electrons [14] leading to diamagnetic byproducts. Such temporal evolutions are very much dependent on the interfacial electron transfer processes. Moreover, this new configuration enables multiple EPR measurements to be carried out using the same covered fiber.

II. Experimental Part

- *Materials and preparation:*

4-hydroxy-2,2,6,6-tetramethylpiperidine 1-oxyl (TEMPOL 97%), Ethylenediaminetetraacetic acid tetrasodium and disodium salts (EDTA) were purchased from Aldrich (France). All these reagents were used as received. MilliQ water (ρ = 18.2 MΩ cm^{-1}) was provide by a Millipore purification system. Aqueous solutions of TEMPOL (100 µM) and EDTA buffer (0.1 M pH 6.5- 7) were prepared. Optical fibers (FG 250 LA) used to support the TiO_2 films were purchased from Thorlabs. They consist of a 250 µm diameter silica glass rod covered with an acrylate cladding. To preserve only the part of the glass rod, 13 cm long pieces were cut and dipped in acetone for 30 min (Carlo Erba). Then, the glass rod pieces were cleaned for 15 min in an ultrasonic bath in a 50/50 ethanol absolute anhydrous (Carlo Erba)/ultrapure water. Heat-shrinkable (700-4532) were purchase from RadioSpares.

- *TiO_2 Deposition Process*

The deposition reactor is an Orion 6 from AJA International with a 2” Ti cathode placed on magnetron sputtering gun. A parametric study was performed to determine the deposition

conditions on polished p-Si (100) (boron doped, Neyco™) and glass-slides substrates (VWR™ microscope slides). These substrates are chosen because of their simple planar geometry which facilitates the coating characterization. In addition, glass-slides are adapted to UV-Visible measurements while Si wafers are adapted to ellipsometry and Fourier transformed Infra-Red spectroscopy.

The chamber was first evacuated down to 10^{-5} mbar at least, before introducing the Argon gas (Alphagaz™). The working pressure was set at 2.2 10^{-3} mbar (argon flowrate at 40 Standard Cubic Centimeters per Minute, sccm). The substrate-target distance is fixed at 138 mm. The DC current mode was used and was set at 400 mA. To deposit titanium oxide thin film, different oxygen flowrates were introduced in the chamber. Since the as-deposited films were amorphous, the as-deposited samples were annealed for 1 h at 520ºC or 720ºC under air atmosphere, with a heating rate of 5ºC/min in a convection furnace from Ceradel.

For the deposition of titanium oxide on the surface of SiO_2 fibers, it was necessary to design and mount a specific fixture. Due the confocal configuration of the deposition system and the small size of the target, the positioning of this fixture was critical in order to obtain homogeneous coating along 4 cm around the center of the fiber. This fixture was composed by two synchronized stepper motors (Nema 14) mounted "face to face" and controlled by an Arduino microcontroller board (Fig. S1). This system was able to ensure a continuous rotation speed (10 rpm) of the fiber under the vapor flux in order to obtain a good radial homogeneity of the thickness.

Thin film characterization:

- X-ray diffraction (XRD) was performed on a Bruker D8 Advance Serie II, with an X-ray source of metallic copper (λ: 1,5406 Å). The acquisition parameters were: scanning of 2θ: 20-60º, a step of 0,05º and acquisition step time of 1,1s. This characterization was performed on the glass-slide samples to avoid the Si peaks from substrate.
- Fourrier-transform infrared (FTIR) spectrometry was performed on Si substrates using a *Nicolet iS 5N* from Thermofisher in transmission mode. The wavenumber scanning range is from 400 to 4000 cm^{-1} with a 2 cm^{-1}resolution.
- X-ray photoelectron spectroscopy (XPS) measurements were performed with a Kratos Axis ultra DLD™ using a monochromatic Al-Kα X-ray source (1486.6 eV) at 180 W. The data acquisition scanning was made from 0.5 to 1200 eV. The acquisition step was 0.5 eV for 100 ms per step.

- Raman spectra were acquired using a Renishaw inVia Reflex spectrometer. The analysis was performed in regular mode using a green laser at a wavelength of 532 nm. The power was 0,4 mW at the sample surface, the magnification was set at x100 with a diffraction grating 2400 holes/mm. This technique confirms the crystallinity of the film on the fiber in a non-destructive way. In fact, calibrating the intensity of the band at 144 cm^{-1} with planar sample helps in the film thickness profile estimation on the fiber. This characterization is made first on the glass-slide substrates, then on the fibers.
- UV-Visible spectroscopy was performed using an UVISEL 1900 from Shimadzu. The measurements are done from 250 nm to 800 nm. This technique allowed to confirm the transparency window of the material and its cutoff wavelength (λcutoff). This characterization was made with the glass-slide substrates.
- Ellipsometry: a Horiba Jobin-Yvon ellipsometer was used with the following acquisition parameters: incidence angle of 70º, scanning from 300 à 850 nm, 300 ms of acquisition time and a 3 nm step. This technique was used to determine de dispersion law of the material by using a-TiO_x (amorphous dispersion) and a multilayer model: one layer of roughness (titanium oxide with some void) / one layer of dense titanium oxide / SiO_2 substrate. DeltaPsi2 was the software used for data treatment.
- Scanning electronic microscopy (SEM): Measurements were performed with a Hitachi SU8010 SEM operated at acceleration voltage of 1 kV.

- *EPR capillaries preparation:*

50 µL glass capillaries (Hirschmann©, *ca.* 1 mm inner diameter) were cut to 7 cm length (using a trim saw Hi-Tech diamond 4''/5''). Labmade pierced stoppers in Polyetheretherketone (PEEK) were manufactured to center the fiber inside the capillaries and validated by tomography (Fig. S2). The step-by-step procedure to prepare a capillary (hereafter designed as the setup) was the following (see detailed schematic description Fig. S3): **i)** the glass fiber is first inserted in one stopper. This assembly is inserted in an empty capillary (without solution) and the second stopper is then positioned. After centering the glass fiber in the capillary, the glass rod fiber is glued (Loctite HY 4070) to one stopper and allowed to stand for 12 hours. **ii)** Once glued, the assembling glass fiber/stopper is removed from both the capillary and the second stopper. **iii)** At this stage, the capillary is filled with 4 cm of the TEMPOL/EDTA solution. The glass fiber/stopper assembly is then reinserted into the filled capillary, taking care to centered the 4 cm solution in relation with the center of the capillary. The second stopper is

then repositioned. **iv)** The two 1 cm long heat-shrinkable parts are positioned and heated (using a heating gun, 150°C) with the filled capillary surrounded by ice (Fig. S4 and S5). **v)** The whole assembly is then suspended from a pendulum mounting using a mandrel. A second weighted mandrel (200 g) is used at the lower end of the fiber to impose tension (Fig. S6). The lower end of the fiber is then glued and allowed to stand for 12 hours to obtain the final setup. The centered position of the fiber is checked by image analysis (Fig. S7). Once the measurements (EPR/illumination) have been taken, the stoppers and the fiber are recovered using chloroform to dissolve the glue and to remove the heat-shrinkable parts. New measurements can then be carried out with the same fiber using a new capillary and new heat-shrinkable parts.

- *Illumination and Electronic paramagnetic Resonance measurements (EPR):*

Continuous-wave EPR X-band spectrometer (EMXplus from Bruker Biospin GmbH, Germany), equipped with a TE-102 resonator, (Bruker) was used to record the fieldswept spectra with the setup described above. The principal experimental parameters values were: a modulation amplitude of 1 G, a microwave power of 4.9 mW, a conversion time constant of *ca.* 12.5 ms, and 5.12 ms time constant. 60 G were swept in 30 s and two scans (2400 points per scan) were accumulated. Illumination of the capillaries was performed outside the cavity using a labmade illumination chamber consisting in 4 UV neon (TL 4) with λ_{max} = 365 nm (*i.e.* 3.4 eV) with an irradiance of *ca.* 1.5 mW·cm^{-2} for a single neon (measured with a power meter 1936-C from Newport). The chamber and the emission spectra of the lamps are presented in Fig. S8. Electronic photo-generation processes occur during the sole irradiation procedure. All experiments were performed at room temperature. A first EPR measurement is performed prior the first irradiation to provide the EPR intensity I_0 at t = 0 s. Then, the following measurements consists of an alternating sequence of illumination step and EPR measurement. EPR intensities were obtained by doubly integrating the low field peak of the TEMPOL EPR signal (Xenon 1.1b.44 Bruker).

- *Tomography:*

Computerized microtomography data were collected on a RXSolutions EasyTom 150-160 tomograph. The tomograph is equipped with a Hamamatsu Open Type Microfocus X-ray source and a VARIAN PaxScan 2520DX detector (1920x1536 pixels on 127 µm pixel pitch, 16-bit). The sample was placed between the source and the detector on a high-resolution rotary stage and moved in order to adjust the resolution to 4µm. The X-ray source was operating at

80kV tube voltage and 30µA tube current. Projections were collected through a helicoidal tomography with 6 rotations composed of 1152 images per rotation (angular increment 0.3125°). Each saved projection is an average of 16 frames captured at 8 frames per second. Filtered backprojection reconstruction using the XAct software from RXSolutions was used to reconstruct the volume. Visualization of the tomograms and measurements were performed using VGSTUDIO MAX software.

III. Results

A. Titanium oxide coatings

Deposition by reactive magnetron sputtering were performed with different oxygen flowrate in the range of 2 to 5 sccm. Ti-O stretching band (432 cm^{-1}) was observed by FTIR for all the samples. Based on XPS measurements, the atomic ration O/Ti was constant and close to 2.3 for all the samples. Even with ion etching before XPS measurement to remove atmospheric pollution, it is possible that some remaining pollution on the surface lead to overestimate the bulk oxygen content. As shown in Fig. 1, the as-deposited coatings were amorphous. One-hour annealing (at 520°C or 720°C) lead to the crystallization of the coatings into the anatase phase (without the presence of rutile diffraction peaks). According to the Tauc plot (Fig. S9A), the annealed coating displays for an indirect band gap a value of 3.26 eV for the anatase phase, which is consistent with reported values [15].

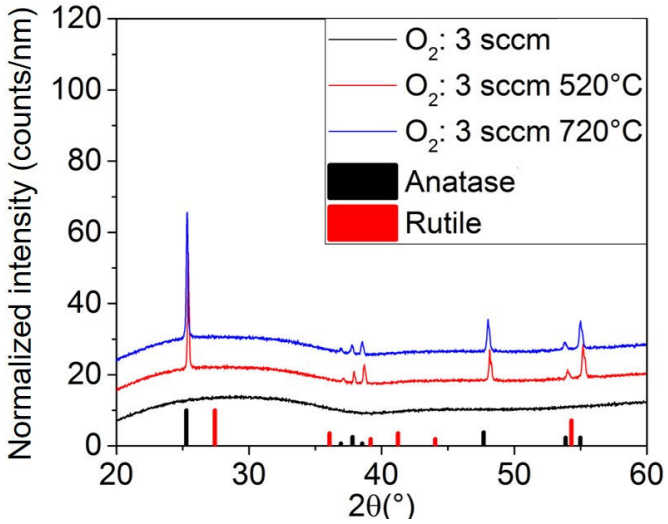

Fig. 1. *XRD diffractograms of thin film without annealing (raw) and at different annealing temperatures synthetized under 3 sccm flow of O_2. Anatase and Rutile bars come from* [16].

Based on preliminary depositions on flat substrate for one hour (thickness obtained by Ellipsometry) and preliminary deposition on the rotating fiber (cross-section observation on SEM), the deposition rate was estimated to 3 nm/min for a fiber rotation at 10 rpm. A deposition time of one hour was then set for all the samples, in order to obtain a coating thickness of 180 nm, over 4 cm around the center of the fiber. The cross-section of the coated fiber observed by SEM presented on Fig. 2 show a homogeneous radial thickness of 172 nm +/- 8 nm, slightly lower than expected. Raman spectra have confirmed the presence of anatase phase (Eg vibration mode at 142, 197 and 636 cm^{-1} [17]) on the fiber after annealing [Fig. 3].

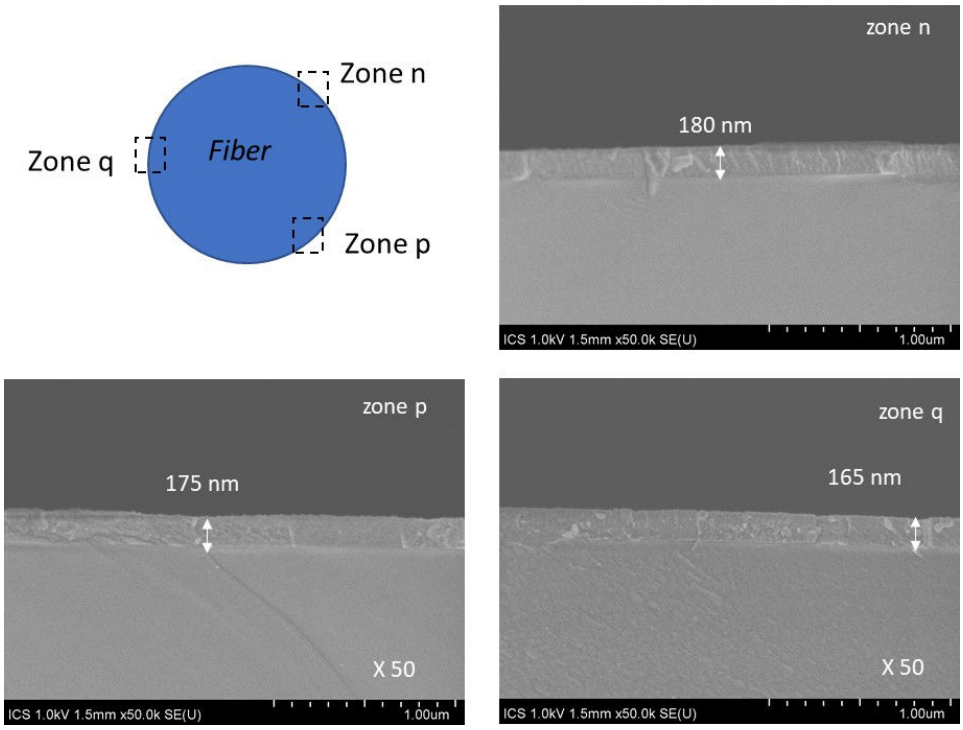

Fig. 2. *Cross section SEM pictures of a glass fiber covered with anatase TiO_2 film.*

The deposition system is thus able to deposit an amorphous TiO_2 continuous layer around the surface of the fiber. The thickness is nearly constant ca. 2.5 % over 4 cm around the center of the length of the fiber (Fig. S10). The thermal treatment is efficient to obtain the crystallization into anatase phase of the coating on the fiber.

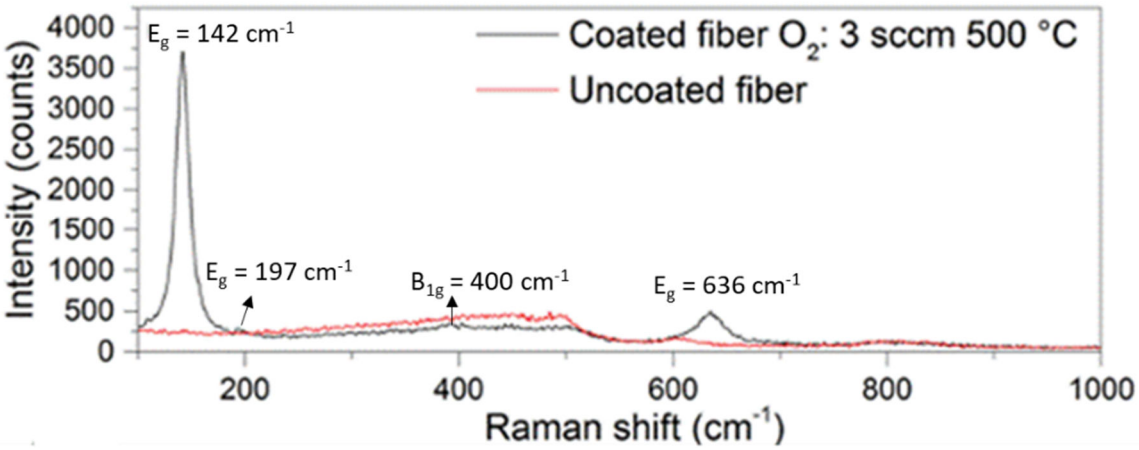

Fig. 3. *Raman spectra of the coated and annealed fiber and an uncoated fiber.*

B. EPR Results

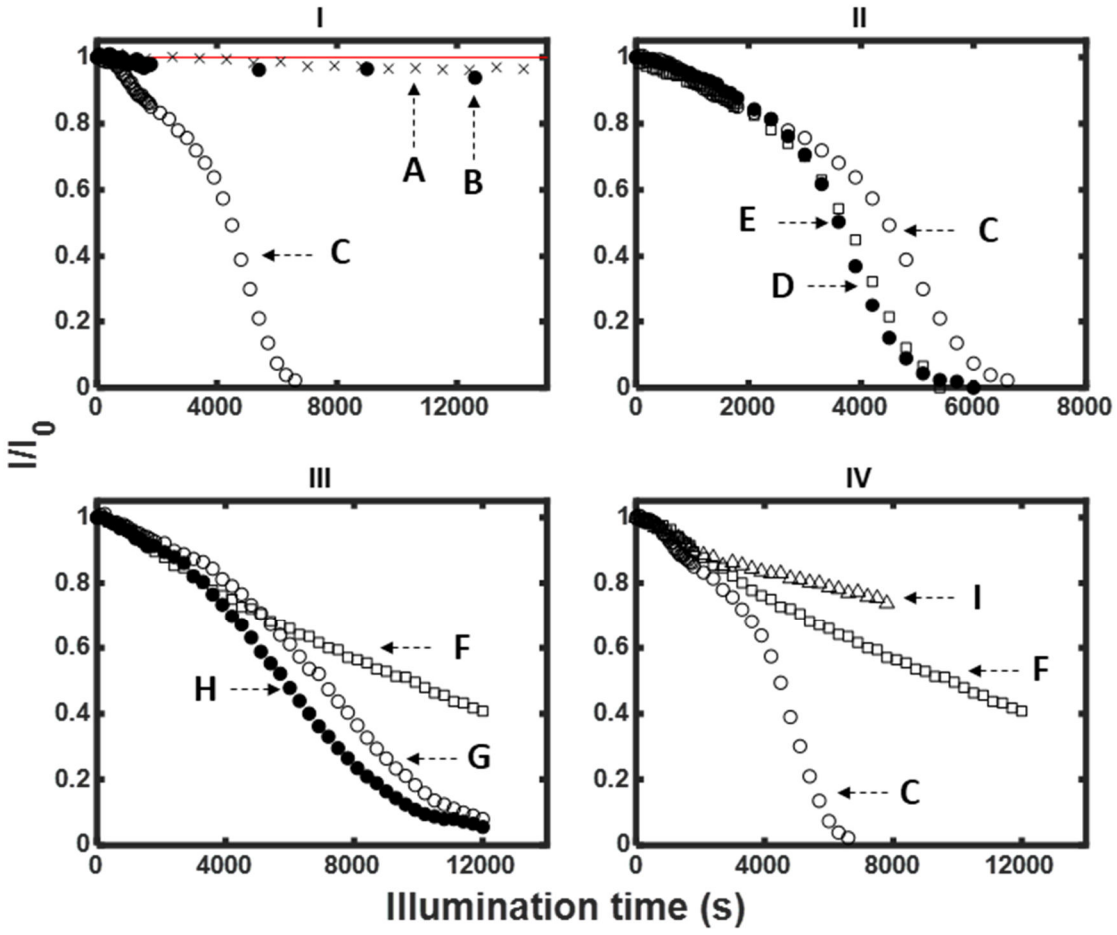

Fig. 4. *Evolution of TEMPOL normalized EPR intensity (I/I_0) with $I_0 = I_{(t=0)}$ as a function of illumination time for:*
***I**: **A)** bare fiber (×), **B)** fiber coated with amorphous TiO_2 (●) and **C)** fiber coated with anatase TiO_2 [a] T measurement 1(○).*
***II**: fiber coated with TiO_2 anatase phase [a] T. **C)** first (○), **D)** second (□) and **E)** third measurement (●).*
***III**: fiber coated with the mixture of TiO_2 anatase phase thickness [b] T: **F)** first measurement 1 (□), **G)** second measurement (○) and **H)** a third measurement with a smaller amount of O_2 (●).*
***IV**: fiber coated with **C)** TiO_2 anatase phase [a] T (○), **F)** the mixture of TiO_2 anatase phase thickness [b] T (□) and **I)** a mixture of TiO_2 anatase phase thickness [c] T (△).*
$[TEMPOL]_{t=0}$ = 0.1 mM, $[EDTA]_{t=0}$ = 1 mM. The solid red line in Fig. I corresponds to $I/I_0 = 1$.

Fig. 4I displays the comparison of the evolution of the TEMPOL EPR intensities as a function of illumination time for a bare fiber (**A**), an amorphous TiO_2 coated fiber (**B**) and an anatase phase TiO_2 coated fiber (**C**). Electron photogeneration is here highlighted for the fiber covered with anatase. Given the illumination energy ($E \approx 3.4$ eV / $\lambda_{max} \approx 365$ nm) and the Energy gaps (E_g) for SiO_2 ($E_g \geq 4$ eV [18] / $\lambda \leq 310$ nm), amorphous TiO_2 ($E_g > 3.2$ eV [19] / $\lambda < 387$ nm,

in this study: $E_g \approx 3.44$ eV/ $\lambda \approx 360$ nm, Fig. S9B) and anatase TiO_2 ($E_g \approx 3.2$ eV [15] / $\lambda \approx 387$ nm), no electron photogeneration is expected for the two first cited. For both the bare fiber and the amorphous TiO_2 coated fiber, a slight similar decreasing compared to $I/I_0 = 1$ (< 5% for illumination time range 0 s-10000 s) in the TEMPOL EPR signal, is nevertheless observed. Further blank experiments *e.g.* setup without fiber using glass and quartz capillaries, showed a similar decay to that in presence of a bare fiber (Fig. S11). The origin of such slight TEMPOL reduction can arise either from an overlap between the neon emission and the TEMPOL absorption (Fig. S12) resulting to photoexcited TEMPOL electrons or the presence of defect in the SiO_2 structure. In presence of EDTA, as sacrificial electron donor, diamagnetic byproduct of TEMPOL can be obtained leading to the slight decay of EPR intensity as a function of illumination time. As part of our goal on modelling the electron photogeneration, this decay represents only a few percent for the first 10000 seconds of illumination and thus is there neglected.

Another prerequisite is to be able to perform a number of experiments with the very same fiber in order to minimize the number of variables and obtain the most accurate comparisons. Fig. 4II presents three measurements carried out with the same fiber covered with TiO_2 anatase phase, that we have named (^{a}T). First measurement (Fig. 4II, curve **C**) corresponds to the first illumination of the fiber just after its preparation, the fiber has never been in contact with any solution under irradiation. The second and third measurements (Fig. 4II, curves **D** and **E**) are the chronological order of fiber reuse. From the experimental evolutions of I/I_0, the second and the third measurements display similar kinetic, yet faster than the first one. Consequently, an initial illumination stage seems to be necessary to optimize the electron photogeneration processes. It can be hypothesized that the density of surface groups such as Ti-OH develops during the first illumination. A similar effect can be then again observed with the same fiber but by changing one parameter. Such setup (^{b}T) differs with (^{a}T) as the fiber is translated in the capillary, always keeping 4 cm of solution TEMPOL/EDTA centered. In this configuration, the photo-probed zone is still made up of anatase phase but, on the 4 cm, around 30% (in length) are anatase that have never been in contact with TEMPOL/EDTA solution. Additionally, instead of having a constant thickness, over the entire length of 4 cm like ^{a}T, there is a thickness gradient as indicated in Fig. S10. Fig. 4III shows the results of two successive measurements with the new fiber configuration consisting in a mixture of TiO_2 anatase phase thickness (^{b}T). As in the previous case with the TiO_2 anatase phase (^{a}T), an evolution of the photoactivity can be clearly observed between the first and the second measurement.

Although it is not possible at present to quantify the various results, several qualitative observations can nevertheless be made. Despite the small surface area of the fiber (≈ 0.315 cm^2) in contact with a solution (in comparison with the use of nanoparticles) and with adequate parameters such as the amount of TEMPOL, a temporal evolution of the photo activity can be obtained within an acceptable range time (a few hours) allowing modelling and quantification during future investigations. The obtained results demonstrate a temporal evolution linked to variations in the semiconducting phase thickness, which will be useful in a context of modelling. As another example, Fig. 4IV displays a comparison of the temporal evolutions of three different probed zones in which the proportion of the TiO_2 anatase phase vary with thinner TiO_2 anatase phase (^{b}T and ^{c}T) when compared to ^{a}T. ^{c}T corresponds here to another translation of the fiber in the capillary (on the 4 cm, around 45 %, in length, are anatase that have never been in contact with TEMPOL/EDTA solution. It appears that the greater the proportion of thinner phase, the lower are the kinetics.

Moreover, evolution of the oxygen concentration can be extracted from the variation of the linewidth (ΔH_{pp}) of the EPR spectra of TEMPOL. Indeed, due to its fundamental triplet state, molecular O_2 is paramagnetic, and leads to dipolar interaction with TEMPOL inducing line broadening of the EPR fingerprint [20]. Indeed, in a fiber free setup, we recorded spectra of TEMPOL 0.1 mM/EDTA 1 mM with (ΔH_{pp} = 1.7 G) and without oxygen (ΔH_{pp} = 1.6 G) after 10 min Ar bubbling. Considering the modulation amplitude equal to 1 G and a linewidth variation of 0.1 G, the evolution of the linewidth with the amount of dioxygen can be monitored. With the exception of one measurement (see below), all the measurements were carried out with solutions prepared under atmospheric condition, *i.e.* in presence of dioxygen (O_2). Fig. 5 shows the partial evolution of the linewidths as a function of illumination time corresponding

to the measurements in Fig. 4. The complete evolutions of the linewidths as a function of illumination time are presented Fig. S13.

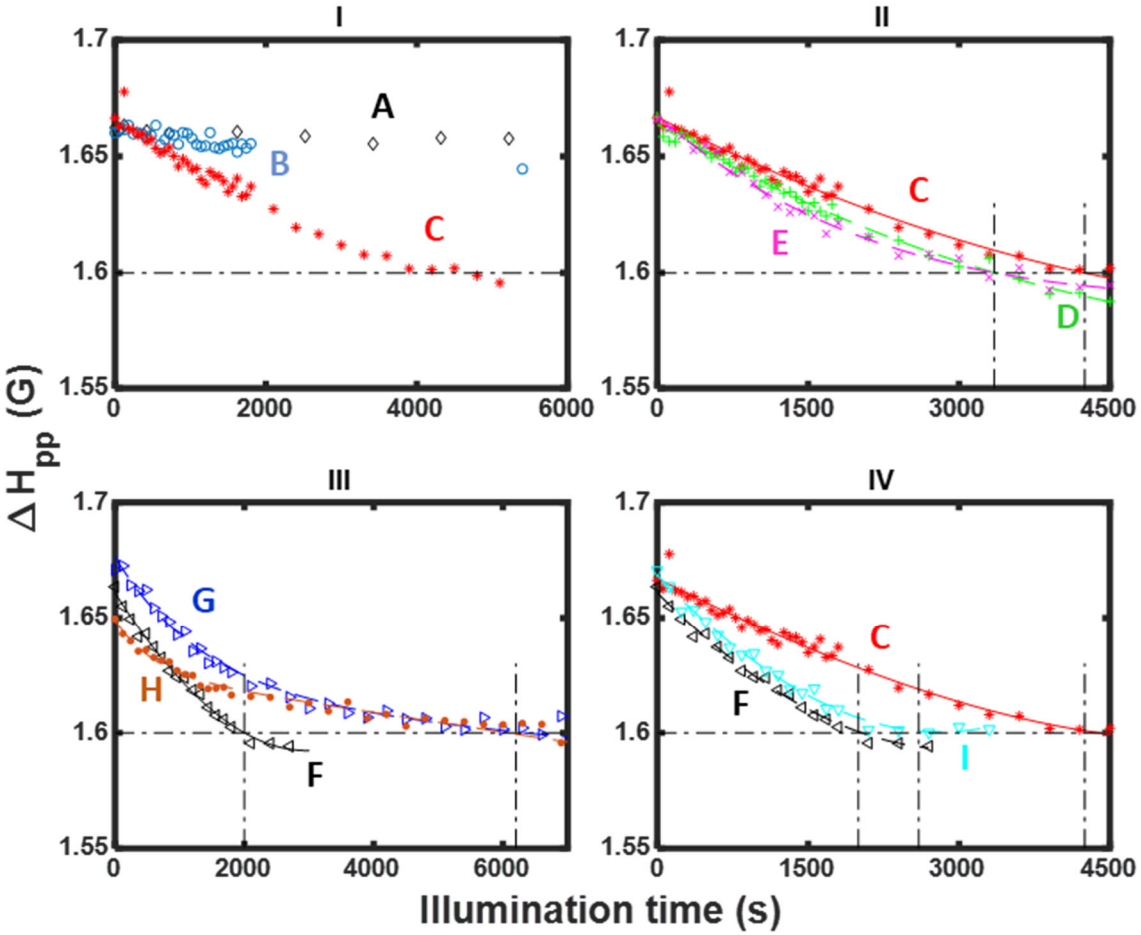

Fig. 5. *Evolutions of TEMPOL low field peak linewidth as a function of time, corresponding to the I/I_0 measurements in Fig. 4, for:*

***I**: (**A**) bare fiber (◇), (**B**) fiber coated with amorphous TiO_2 (○) and (**C**) fiber coated with TiO_2 anatase phase [a] T (✳). Corresponding to Fig. 4I*

***II**: fiber coated with TiO_2 anatase phase [a] T. **C**) first (✳), **D**) second (+) and **E**) third measurement (×). Corresponding to Fig. 4II*

***III**: fiber coated with the mixture of TiO_2 anatase phase thickness [b] T: **F**) first measurement (◁), **G**) second measurement (▷) and **H**) a third measurement with a smaller amount of O_2 (●). Corresponding to Fig. 4III*

***IV**: fiber coated with **C**) TiO_2 anatase phase [a] T (✳), **F**) the mixture of TiO_2 anatase phase thickness [b] T (◁) and **I**) a mixture of TiO_2 anatase phase thickness [c] T (▽). Corresponding to Fig. 4IV*

Except the horizontal dash-dotted line that indicates the linewidth value of 1.6 G, all the lines shall guide the eye. The vertical lines indicate the time intersection with the linewidth value of 1.6 G. $[TEMPOL]_{t=0}$ = 0.1 mM, $[EDTA]_{t=0}$ = 1 mM.

For the setup with bare fiber or fiber coated with amorphous TiO_2, as well as the corresponding EPR intensity, low field peak ΔH_{pp} of TEMPOL seems to be independent of the illumination time, thus confirming the absence of electron photogeneration. Quite opposite, the fiber coated with the TiO_2 anatase phase ([a]T) exhibits a reproducible decay of ΔH_{pp} from 1.67 G to 1.60 G,

where the latter value points towards absence of O_2. Hence, the evolution of the EPR linewidth combined with the evolution of TEMPOL EPR intensity, is pertinent for mechanistic modelling as it probes molecular oxygen, that competes with TEMPOL during electron photogeneration. Indeed, differences can be observed with the anatase phase of TiO_2 depending on the ranking of the measurement. The evolutions of the linewidths corresponding to the first, second and third measurements (Fig. 4II) are presented in Fig. 5II. Indeed, the illumination time required to deplete molecular oxygen from the solution (*i.e.* TEMPOL ΔH_{pp} = 1.60 G) is reduced of *ca.* 20% between the first (**C**) and second (**D**) measurement, pointing to changes in the kinetic processes.

Interestingly, opposite variation is observed with the inhomogeneous thickness zone of TiO_2 anatase phase (^{b}T). The O_2 consumption appears faster for the first measurement **F** than for the second **G** (Fig. 5III) whereas the corresponding TEMPOL I/I_0 evolutions are slower (Fig. 5III). This trend is confirmed if we consider ^{a}T and the two different phase mixtures of TiO_2 anatase (^{b}T and ^{c}T, Fig. 5IV). The TEMPOL reduction over illumination time slows down while the depletion of O_2 is faster for the two mixtures of TiO_2 anatase phase thickness. Noteworthy, with a single experiment, it is possible to collect kinetic information on both TEMPOL and O_2, as function of several parameters. Therefore, charge transfer processes, a crucial issue for the optimization of application devices, can be pointed out. On the one side, TEMPOL can be reduced by a proton radical [13] and electrochemically [14]. Thus, the assumption of direct and indirect charge transfer processes [12,21] should depend on interface properties. On the other side, it is accepted that the reduction of O_2 requires direct electron transfer [22]. Assuming that these kinetic processes depend only on the surface density groups, indirect electron transfer (producing radicals) are more probable in area with higher density while direct electron transfer are favored in lower ones. By combining the TEMPOL I/I_0 and linewidth kinetics it should be possible to obtained parameters for each mechanism. Yet, whether the components receiving the photogenerated electrons affect the surface composition remains an open question.

In order to bring additional relevant information, it would also be necessary to perform measurements with TEMPOL, in anaerobic conditions. Nevertheless, preparing a complete O_2 free setup is not straightforward. However, a first attempt has been performed by bubbling the TEMPOL/EDTA solution aqueous solution with Ar (15 min) prior to build up the setup under Ar flow. The results are provided Fig. 4III for the evolution I/I_0 and Fig. 5III for the evolution of the linewidths. The linewidth is linear as a function of the amount of O_2 [20]. So, an initial linewidth equal to 1.64 G points to *ca.* 40% O_2 decay compared to standard oxygenated

condition. While, a faster kinetic of TEMPOL reduction is observed when compared with former experiments under aerobic condition (Fig. 4III), a sigmoidal shape is nevertheless obtained testimony of the competition between O_2 and TEMPOL as photo-electron scavenger. This points towards the limit of the actual procedure and will improve in future investigations.

III. Conclusion

This study presents the basis of a new approach, based on Electron Paramagnetic Resonance (EPR), to investigate the photogenerated charge transfer processes at the interface semiconductor (SC)/water. A simple study object has been developed to suit EPR measurements, electron photogenerated and future quantification and modeling. Glass fibers, of 250 µm diameter were covered with a thin film of ca. 200 nm of amorphous or anatase phase of titanium oxide (TiO_2), were inserted and centered in capillaries of 1 mm diameter. This developed configuration allows to reuse the same object for multiple measurements, tracking the time evolution of a probe molecule's paramagnetic signal intensity and the linewidth to obtain concomitant and independent information about the temporal evolution of the dioxygen amount as a function of illumination time. Thus, clear difference in temporal evolutions was measured between the first and subsequent illumination steps, which would suggest a likely change of the surface groups. Additionally, combining EPR intensity and linewidth evolutions, it becomes possible to define the presence of dioxygen even when the variation in its quantity is no important. This new approach, open to all semiconductors, should provide trustworthy information for a better understanding of charge transfers at the SC/water interface and help overcome limitations for the development of efficient devices for dihydrogen photogeneration.

Acknowledgements

We thank Damien Favier for tomographic measurements, traction tests and the MINAMEC platform of ICS. We also thank Alain Carvalho for SEM measurements and the PLAMICS microscopy facility of ICS for technical support and the use of their equipment.

References

[1] S. Ali, P. M. Ismail, M. Khan, A. Dang, S. Ali, A. Zada, F. Raziq, I. Khan, M. S. Khan, M. Ateeq, W. Khan, S. H. Bakhtiar, H. Ali, X. Wu, M. I. A. Shah, A. Vinu, J. Yi, P. Xia, and L. Qiao, Charge transfer in TiO2-based photocatalysis: fundamental mechanisms to material strategies, *Nanoscale* 16 (2024) 4352.

[2] F. d'Amore, A. Nava, P. Colbertaldo, C. G. Visconti, and M. C. Romano, Turning CO_2 from fuel combustion into e-Fuel? Consider alternative pathways, *Energy Convers. Manag.* 289 (2023) 117170.

[3] A. Fujishima and K. Honda, Electrochemical Photolysis of Water at a Semiconductor Electrode, *Nature* 238 (1972) 37.

[4] D.-E. Lee, M.-K. Kim, M. Danish, and W.-K. Jo, State-of-the-art review on photocatalysis for efficient wastewater treatment: Attractive approach in photocatalyst design and parameters affecting the photocatalytic degradation, *Catal. Commun.* 183 (2023) 106764.

[5] M. A. Hassaan, M. A. El-Nemr, M. R. Elkatory, S. Ragab, V.-C. Niculescu, and A. El Nemr, Principles of Photocatalysts and Their Different Applications: A Review, *Top. Curr. Chem.* 381 (2023) 31.

[6] I. Ahmad, Y. Zou, J. Yan, Y. Liu, S. Shukrullah, M. Y. Naz, H. Hussain, W. Q. Khan, and N.R. Khalid, Semiconductor photocatalysts: A critical review highlighting the various strategies to boost the photocatalytic performances for diverse applications, *Adv. Colloid Interface Sci.* 311 (2023) 102830.

[7] S. Gelin, N. E. Kirchner-Hall, R. R. Katzbaer, M. J. Theibault, Y. Xiong, W. Zhao, M. M. Khan, E. Andrewlavage, P. Orbe, S. M. Baksa, M. Cococcioni, I. Timrov, Q. Campbell, H. Abruña, R. E. Schaak, and I. Dabo, Ternary Oxides of *s*- and *p*-Block Metals for Photocatalytic Solar-to-Hydrogen Conversion, *PRX Energy* 3 (2024) 013007.

[8] V. Sharma, B. Bein, A. Lai, B. Pamuk, C. E. Dreyer, M. Fernández-Serra, and M. Dawber, Cooperative Interactions between Surface Terminations Explain Photocatalytic Water Splitting Activity on SrTiO3, *PRX Energy* 1 (2022) 023002.

[9] X. Wang and C. Li, Interfacial charge transfer in semiconductor-molecular photocatalyst systems for proton reduction, *J. Photochem. Photobiol. C: Photochem. Rev.* 33 (2017) 165.

[10] S. Kumar, K. Ojha, and A. K. Ganguli, Interfacial Charge Transfer in Photoelectrochemical Processes *Adv. Matter. Interfaces* 4 (2017) 1600981.

[11] M. Twardoch, Y. Messai, B. Vileno, Y. Hoarau, D. E. Mekki, O. Felix, P. Turek, J. Weiss, G. Decher, and D. Martel, Development of an electron paramagnetic resonance methodology for studying the photogeneration of reactive species in semiconductor nano-particle assembled films, *Mol. Phys.* 116 (2018) 1558.

[12] D. Martel, A. Guerra, P. Turek, J. Weiss, and B. Vileno, Pertinent parameters in photo-generation of electrons: Comparative study of anatase-based nano-TiO_2 suspensions, *J. Coll. Inter. Sci.* 467 (2016) 300.

[13] K.-I. Matsumoto, K. Nagata, H. Yamamoto, K. Endo, K. Anzai, and I. Aoki, Visualization of free radical reactions in an aqueous sample irradiated by 290 MeV carbon beam, *Magn. Reson. Med.* 61 (2009) 1033.

[14] Y. Kato, Y. Shimizu, L. Yijing, K. Unoura, H. Utsumi, and T. Ogata, Reversible half-wave potentials of reduction processes on nitroxide radicals, *Electrochim. Acta* 40 (1995) 2799.

[15] D. Reyes-coronado, G. Rodríguez-Gattorno, M. E. Espinosa Pesqueira, C. Cab, R. de Coss, and G. Oskam, Phase-pure TiO_2 nanoparticles: anatase, brookite and rutile, *Nanotechnology* 19 (2008) 145605.

[16] A. N. Banerjee, The design, fabrication, and photocatalytic utility of nanostructured semiconductors: focus on TiO2-based nanostructures, *Nanotechnol. Sci. Appl.* 4 (2011) 35.

[17] T. Ohsaka, F. Izumi, and Y. Fujiki, Raman spectrum of anatase, TiO_2, *J. Raman Spectrosc.* 7 (1978) 321.

[18] R. H. French, R. Abou-Rahme, D. j. Jones, L. E. McNeil, Absorption Edge and band gap of SiO_2 fused silica glass, *Ceramic Transactions* 28 (1992) 63.

[19] J. Liang, N. Wang, Q. Zhang, B. Liu, X. Kong, C. Wei, D. Zhang, B. Yan, Y. Zhao, and X. Zhang, Exploring the mechanism of a pure and amorphous black-blue TiO2:H thin film as a photoanode in water splitting *Nano Energy* 42 (2017) 151.

[20] R. Ahmad and P. Kuppusamy, Theory, Instrumentation, and Applications of EPR Oximetry, *Chem. Rev.* 110 (2010) 3212.

[21] T. Lana Villarreal, R. Gómez, M. Neumann-Spallart, N. Alonso-Vante, and P. Salvador, Semiconductor Photooxidation of Pollutants Dissolved in Water: A Kinetic Model for Distinguishing between Direct and Indirect Interfacial Hole Transfer. I. Photoelectrochemical Experiments with Polycrystalline Anatase Electrodes under Current Doubling and Absence of Recombination, *J. Phys. Chem. B* 108 (2004) 15172.

[22] D.-E. Lee, M.-K. Kim, M. Danish, and W.-K. Jo, State-of-the-art review on photocatalysis for efficient wastewater treatment: Attractive approach in photocatalyst design and parameters affecting the photocatalytic degradation, *Catal. Commun.* 183 (2023) 106764.